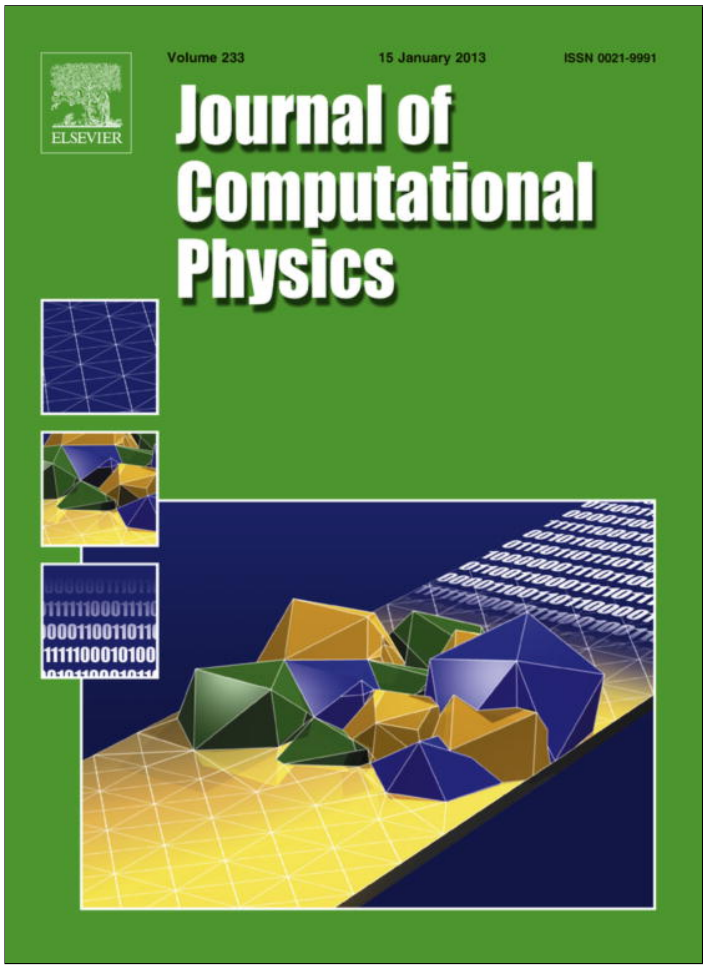

Journal of Computational Physics 233 (2013) 509–526

Contents lists available at SciVerse ScienceDirect

Journal of Computational Physics

journal homepage: www.elsevier.com/locate/jcp

Numerical simulation of the impact and deposition of charged particulate droplets

T.I. Zohdi *

Department of Mechanical Engineering, 6195 Etcheverry Hall, University of California, Berkeley, CA 94720-1740, USA

ARTICLE INFO

Article history:
Received 9 January 2012
Received in revised form 4 September 2012
Accepted 10 September 2012
Available online 25 September 2012

Keywords:
Staggering scheme
Charged particulates
Clusters
Impact

ABSTRACT

This work addresses the impact and deposition of charged "cluster-droplets", comprised of particulates, on electrified surfaces. A direct numerical method is developed, based on an implicit, staggered, time-stepping scheme which separates the impulsive and continuous forces between particles, in conjunction with an iterative solution method that automatically adapts the time-step sizes to control the rates of convergence within a time-step. This approach is used to investigate the post-impact structure of charged particulate cluster-droplets. Particulate cluster-droplet impact has wide-ranging application to areas such as inkjet printing, sprays, coatings, etc. A series of numerical examples are provided, where we investigate the effect of progressively increasing the electric field strength on the impacted substrate, leading to a more coherent cluster deposition. An analysis is also provided for the interaction of charged cluster-droplets with electromagnetic fields.

1. Introduction

The focus of this work is the numerical simulation of the dynamics of collections of charged particles, initially in the form of "cluster-droplets", and the resulting impact behavior of such clusters on electrified surfaces. An overall model, amenable to numerical simulation, is constructed by assembling submodels of the multistage physical events in order to form a system that is solved numerically, in a staggered manner. Specifically, a numerical strategy is developed whereby the dynamics of charged particles, accounting for their collisions, inter-particle near-fields, interaction with external electromagnetic fields are all computed implicitly in an iterative, modular, manner. The numerical approach is based on an implicit, staggered, time-stepping scheme that separates the impulsive and continuous forces between particles, in conjunction with an iterative solution method that automatically adapts the time step sizes to control the rates of convergence within the time step.

The coherency of an impacting cluster-droplet is of particular interest, and has wide-ranging application to inkjet printing, sprays, coatings, etc. A central issue is the determination of the electrical field strength on the surface, which leads to a coherent droplet deposition, versus a droplet that will break apart. The present analysis is partially motivated by coating technologies (for example epitaxy and electrostatic painting) that ionize particulates and electrify surfaces to capture the particles, in order to enhance the quality of coating. Relative to a charge-free and electric-field-free system, the resulting coatings can be more accurately controlled, provided the system parameters are appropriately set. The presentation is broken into three main parts: (1) modeling of large aggregates of particles forming a cluster-droplet, (2) numerical methods for a collection of charged particles and (3) numerical examples of cluster-surface impact.

* Tel.: +1 510 642 9172; fax: +1 510 642 6163.
E-mail address: zohdi@me.berkeley.edu

0021-9991/$ - see front matter © 2012 Elsevier Inc. All rights reserved.
http://dx.doi.org/10.1016/j.jcp.2012.09.012

Remarks. The presented work is motivated by the industrial need for numerical simulation of a variety of coating deposition techniques that employ aspects of charged-particles and electromagnetic fields. The particles are endowed with charges through a variety of possible methods, such as: (1) Post-atomization charging-whereby the particles come into contact with an electrostatic field (produced by electrostatic induction or by electrodes) downstream of the outlet nozzle, (2) Direct charging-whereby an electrode is immersed in the coating supply and (3) Tribological charging-whereby the friction in the nozzle induces an electrostatic charge on the particles as they rub the surface. There are a large variety of industrial deposition techniques, and we refer the reader to the surveys of the state of the art found in Martin [31,32]. Beyond the previously mentioned applications, there are a variety of other areas where cluster of particulates arise, such as small-scale manufacturing processes (see, for example, Luo and Dornfeld [27–30], Arbelaez et al. [1,2], Ciampini et al. [6,7], Gomes-Ferreira et al. [20], Ghobeity et al. [16,17], Choi et al. [3–5] and Demko et al. [8]). Improper handling of these clusters can lead to manufacturing inconsistencies/variability which can strongly affect the overall product quality, in particular if the manufactured devices have small dimensions. For a review of the effects of clusters on the macroscale material properties of solids that contain them, see Torquato [42], as well as Ghosh et al. [18] for domain partitioning methods that are capable of handling materials with general nonuniform microstruture.

2. Multiple particulate systems in the presence of near-fields

As mentioned in the introduction, we are concerned with the dynamics of charged cluster-droplets, formed by groups of particulates, when they impact a surface possessing an electric field. In particular, the coherency of the resulting impacted cluster-droplet is of interest (Fig. 1). For a droplet comprised of multiple interacting particles, we must resort to numerical procedures. *The objects in the system are assumed to be small enough to be considered* (*idealized*) *as particles, spherical in shape, and that the effects of their rotation with respect to their mass center is unimportant to their overall motion.*

We consider a group of non-intersecting particles (N_p in total) and build on the previous works of Zohdi [47–54]. The equation of motion for the *ith* particle in a flow is

$$m_i \ddot{\boldsymbol{r}}_i = \boldsymbol{\Psi}_i^{tot}(\boldsymbol{r}_1, \boldsymbol{r}_2, \ldots, \boldsymbol{r}_{N_p}) = \boldsymbol{\Psi}_i^{nf} + \boldsymbol{\Psi}_i^{con} + \boldsymbol{\Psi}_i^{fric} + \boldsymbol{\Psi}_i^{env}, \tag{2.1}$$

where $\boldsymbol{r}_i$ is the position vector of the *ith* particle and where $\boldsymbol{\Psi}_i^{tot}$ represents all forces acting on particle i, which is decomposed into the sum of forces due to near-field interaction, $\boldsymbol{\Psi}_i^{nf}$, where we use a simple *empirical* interaction law that is of the form:

$$\boldsymbol{\Psi}_i^{nf} = \sum_{j \neq i}^{N_p} \left(\underbrace{\alpha_{1ij} ||\boldsymbol{r}_i - \boldsymbol{r}_j||^{-\beta_1}}_{\text{attraction}} - \underbrace{\alpha_{2ij} ||\boldsymbol{r}_i - \boldsymbol{r}_j||^{-\beta_2}}_{\text{repulsion}} \right) \underbrace{\boldsymbol{n}_{ij}}_{\text{unit vector}}, \tag{2.2}$$

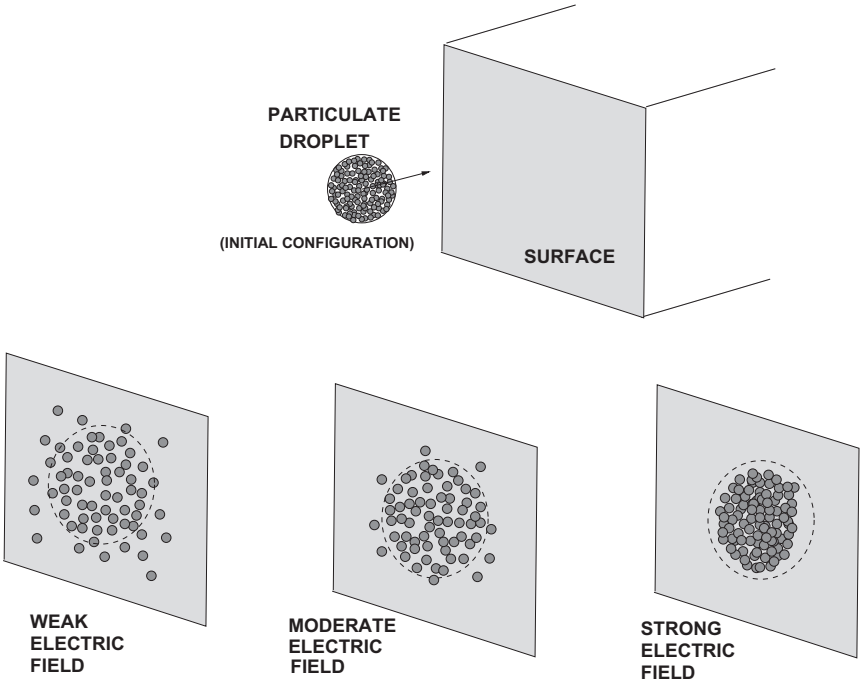

Fig. 1. Particulate cluster-droplet behavior as a function of the surface (attractive) electric field.

where the α's and β's are empirical material parameters and $\boldsymbol{n}_{ij}$ is the normal direction, determined by the difference in the position vectors of the particles' centers, defined by

$$\boldsymbol{n}_{ij} \stackrel{\text{def}}{=} \frac{\boldsymbol{r}_j - \boldsymbol{r}_i}{||\boldsymbol{r}_i - \boldsymbol{r}_j||}, \tag{2.3}$$

where $||\boldsymbol{r}_i - \boldsymbol{r}_j||$ is the separation distance between particle i (located at $\boldsymbol{r}_i$) and j (located at $\boldsymbol{r}_j$) and $||\cdot||$ represents the Euclidean norm in R^3. We note that there are a variety of possible interparticle near-field representations for charged particles, such as Eq. 2.2. We refer the reader to Frenklach and Carmer [15], Haile [24], Hase [23], Rapaport [34], Torquato [43], Rechtsman et al. [35,36] and Zohdi [47–54] for overviews of the various representations for particle interaction, such as those based on the familiar Mie, Lennard–Jones, and Morse potentials (see Moelwyn-Hughes [33] for reviews). Also, three-body terms can be introduced directly into the inter-particle interaction (Stillinger [38]) or via term-wise modifications to the two-body representations (Tersoff [41]). The external electromagnetic fields are accounted via $\boldsymbol{\Psi}_i^{env} = q_i(\boldsymbol{E}^{ext} + \boldsymbol{v}_i \times \boldsymbol{B}^{ext})$, where q_i is the effective (overall) charge of the particle i. $\boldsymbol{E}^{ext}$ and $\boldsymbol{B}^{ext}$ are externally-controlled fields that are independent of the response of the system. $\boldsymbol{E}^{ext}$ and $\boldsymbol{B}^{ext}$ can be considered as static (or extremely slowly-varying), and thus mutually uncoupled and independently controllable. The normal contact impulsive forces ($\boldsymbol{\Psi}_i^{con}$), frictional impulse forces ($\boldsymbol{\Psi}_i^{fric}$) are discussed next.

Remarks. In order to motivate the near-field empirical interaction formulation, we recall that the force between two ions is given by (Coulomb's law)

$$\boldsymbol{\Psi}_{ij}^{e} = \frac{q_i q_j}{4\pi\epsilon||\boldsymbol{r}_i - \boldsymbol{r}_j||^2}\boldsymbol{n}_{ij} \tag{2.4}$$

where $\boldsymbol{\Psi}_{ij}^{e}$ is the force acting between the particles, q_i is the charge of particle i, q_j is the charge of particle j and ϵ is the permittivity. Usually, one writes $\epsilon = \epsilon_o\epsilon_r$ where $\epsilon_o = 8.854 \times 10^{-12}$ F/m is the free space permittivity and ϵ_r is the relative permittivity or "dielectric" constant. For point charges of like sign, the Coulombic force is one of repulsion, while for opposite charges the force is attractive. When we consider particles that have been ionized, they are not a result of a single charge, but a collection of many ions that are tightly bound together, for example a positively-charged core of material with negative charged smaller-scale ions surrounding the core or vice versa, a negative core with positive ions surrounding the core. Of course, there can be many other possible positive–negative combinations. Theoretically speaking, Maxwell's equations could be applied at the scale of each charged domain within a collection of charged particulates, however, the system of equations would become quite complex and enormous. For this reason, empirically-generated effective interaction laws for complex charged-particulate interaction, which possess attractive and repulsive components, are employed components. As indicated, the specific structure of the near-field interaction law chosen was only one of many possibilities to model near-field behavior. There are vast numbers of empirical representations, for example, found in the field of "Molecular Dynamics" (MD), which typically refers to mathematical models of systems of atoms or molecules where each atom (or molecule) is represented by a material point in R^3 and is treated as a point mass. The overall motion of such mass-point systems is dictated by Newtonian mechanics. For an extensive survey of MD-type interaction forces, which includes comparisons of the theoretical and computational properties of a variety of interaction laws, we refer the reader to Frenklach and Carmer [15].

3. Mechanical contact with near-field interaction

We consider cases where mechanical contact occurs between particles, in the presence of near-field interaction. A primary simplifying assumption is made: *the particles remain spherical after impact, i.e. any permanent deformation is considered negligible*.

3.1. Contact and momentum exchange

Following Zohdi [48,50,54], for two colliding particles i and j, normal to the line of impact, a balance of linear momentum relating the states before impact (time = t) and after impact (time = $t + \delta t$) reads as

$$m_i v_{in}(t) + m_j v_{jn}(t) + \int_t^{t+\delta t} \mathcal{E}_i \cdot \boldsymbol{n}_{ij}\, dt + \int_t^{t+\delta t} \mathcal{E}_j \cdot \boldsymbol{n}_{ij}\, dt = m_i v_{in}(t+\delta t) + m_j v_{jn}(t+\delta t), \tag{3.1}$$

where the subscript n denotes the normal component of the velocity (along the line connecting particle centers) and the $\mathcal{E}$'s represent all forces induced by near-field interaction with other particles, as well as all other external forces, if any, applied to the pair. If one isolates one of the members of the colliding pair, then

$$m_i v_{in}(t) + \int_t^{t+\delta t} I_n\, dt + \int_t^{t+\delta t} \mathcal{E}_i \cdot \boldsymbol{n}_{ij}\, dt = m_i v_{in}(t+\delta t), \tag{3.2}$$

where $\int_t^{t+\delta t} I_n\, dt$ is the total normal impulse due to impact. For a pair of particles undergoing impact, let us consider a decomposition of the collision event into a compression (δt_1) and recovery (δt_2) phase, i.e. $\delta t = \delta t_1 + \delta t_2$. Between the compression

and recovery phases, the particles achieve a common normal velocity,[1] denoted v_{cn}, at the intermediate time $t+\delta t_1$. We may write for particle i, along the normal, in the compression phase of impact

$$m_i v_{in}(t) + \int_t^{t+\delta t_1} I_n \, dt + \int_t^{t+\delta t_1} \mathcal{E}_i \cdot \boldsymbol{n}_{ij} \, dt = m_i v_{cn}, \tag{3.3}$$

and in the recovery phase

$$m_i v_{cn} + \int_{t+\delta t_1}^{t+\delta t} I_n \, dt + \int_{t+\delta t_1}^{t+\delta t} \mathcal{E}_i \cdot \boldsymbol{n}_{ij} \, dt = m_i v_{in}(t+\delta t). \tag{3.4}$$

For the other particle (j), in the compression phase,

$$m_j v_{jn}(t) - \int_t^{t+\delta t_1} I_n \, dt + \int_t^{t+\delta t_1} \mathcal{E}_j \cdot \boldsymbol{n}_{ij} \, dt = m_j v_{cn}, \tag{3.5}$$

and in the recovery phase

$$m_j v_{cn} - \int_{t+\delta t_1}^{t+\delta t} I_n \, dt + \int_{t+\delta t_1}^{t+\delta t} \mathcal{E}_j \cdot \boldsymbol{n}_{ij} \, dt = m_j v_{jn}(t+\delta t). \tag{3.6}$$

This leads to an expression for the coefficient of restitution

$$e \overset{\text{def}}{=} \frac{\int_{t+\delta t_1}^{t+\delta t} I_n \, dt}{\int_t^{t+\delta t_1} I_n \, dt} = \frac{m_i(v_{in}(t+\delta t) - v_{cn}) - \mathcal{E}_{in}(t+\delta t_1, t+\delta t)}{m_i(v_{cn} - v_{in}(t)) - \mathcal{E}_{in}(t, t+\delta t_1)} = \frac{-m_j(v_{jn}(t+\delta t) - v_{cn}) + \mathcal{E}_{jn}(t+\delta t_1, t+\delta t)}{-m_j(v_{cn} - v_{jn}(t)) + \mathcal{E}_{jn}(t, t+\delta t_1)}, \tag{3.7}$$

where

$$\begin{aligned}
\mathcal{E}_{in}(t+\delta t_1, t+\delta t) &\overset{\text{def}}{=} \int_{t+\delta t_1}^{t+\delta t} \mathcal{E}_i \cdot \boldsymbol{n}_{ij} \, dt, \\
\mathcal{E}_{jn}(t+\delta t_1, t+\delta t) &\overset{\text{def}}{=} \int_{t+\delta t_1}^{t+\delta t} \mathcal{E}_j \cdot \boldsymbol{n}_{ij} \, dt, \\
\mathcal{E}_{in}(t, t+\delta t_1) &\overset{\text{def}}{=} \int_{t}^{t+\delta t_1} \mathcal{E}_i \cdot \boldsymbol{n}_{ij} \, dt, \\
\mathcal{E}_{jn}(t, t+\delta t_1) &\overset{\text{def}}{=} \int_{t}^{t+\delta t_1} \mathcal{E}_j \cdot \boldsymbol{n}_{ij} \, dt.
\end{aligned} \tag{3.8}$$

If we eliminate v_{cn}, we obtain an expression for e

$$e = \frac{v_{jn}(t+\delta t) - v_{in}(t+\delta t) + \Delta_{ij}(t+\delta t_1, t+\delta t)}{v_{in}(t) - v_{jn}(t) + \Delta_{ij}(t, t+\delta t_1)}, \tag{3.9}$$

where[2]

$$\Delta_{ij}(t+\delta t_1, t+\delta t) \overset{\text{def}}{=} \frac{1}{m_i}\mathcal{E}_{in}(t+\delta t_1, t+\delta t) - \frac{1}{m_j}\mathcal{E}_{jn}(t+\delta t_1, t+\delta t) \tag{3.11}$$

and

$$\Delta_{ij}(t, t+\delta t_1) \overset{\text{def}}{=} \frac{1}{m_i}\mathcal{E}_{in}(t, t+\delta t_1) - \frac{1}{m_j}\mathcal{E}_{jn}(t, t+\delta t_1). \tag{3.12}$$

Thus, we may rewrite Eq. (3.9) as

$$v_{jn}(t+\delta t) = v_{in}(t+\delta t) - \Delta_{ij}(t+\delta t_1, t+\delta t) + e\big(v_{in}(t) - v_{jn}(t) + \Delta_{ij}(t, t+\delta t_1)\big). \tag{3.13}$$

It is convenient to denote the average force acting on the particle from external sources as

$$\overline{\mathcal{E}}_{in} \overset{\text{def}}{=} \frac{1}{\delta t}\int_t^{t+\delta t} \mathcal{E}_i \cdot \boldsymbol{n}_{ij} \, dt. \tag{3.14}$$

If e is explicitly known, then one can write, combining Eqs. (3.9) and (3.1)

[1] A common normal velocity for particles should be interpreted as indicating that the relative velocity in the normal direction between particle centers is zero.

[2] This collapses to the classical expression for the ratio of the relative velocities before and after impact, if the near-field forces are negligible:

$$e \overset{\text{def}}{=} \frac{v_{jn}(t+\delta t) - v_{in}(t+\delta t)}{v_{in}(t) - v_{jn}(t)}. \tag{3.10}$$

$$v_{in}(t+\delta t) = \frac{m_i v_{in}(t) + m_j(v_{jn}(t) - e(v_{in}(t) - v_{jn}(t)))}{m_i + m_j} + \frac{(\overline{\mathcal{E}}_{in} + \overline{\mathcal{E}}_{jn})\delta t - m_j(e\Delta_{ij}(t, t+\delta t_1) - \Delta_{ij}(t+\delta t_1, t+\delta t))}{m_i + m_j}, \tag{3.15}$$

and, once $\boldsymbol{v}_{in}(t+\delta t)$ is known, one can subsequently also solve for $v_{jn}(t+\delta t)$ via Eq. (3.13).

Remark 1. Later, it will be useful to define the average impulsive normal contact force between the particles acting during the impact event as

$$\bar{I}_n \overset{\text{def}}{=} \frac{1}{\delta t}\int_t^{t+\delta t} I_n\, dt = \frac{m_i(v_{in}(t+\delta t) - v_{in}(t))}{\delta t} - \overline{\mathcal{E}}_{in}. \tag{3.16}$$

In particular, as will be done later in the analysis, when we discretize the equations of motion with a discrete (finite difference) time-step of Δt, where $\delta t \ll \Delta t$, we shall define the impulsive normal contact contribution to the total force acting on a particle, $\boldsymbol{\Psi}_i^{tot} = \boldsymbol{\Psi}_i^{nf} + \boldsymbol{\Psi}_i^{con} + \boldsymbol{\Psi}_i^{fric} + \boldsymbol{\Psi}_i^{env}$ (Eq. 2.1), to be

$$\boldsymbol{\Psi}_i^{con} = \frac{\bar{I}_n \delta t}{\Delta t}\boldsymbol{n}_{ij}. \tag{3.17}$$

Furthermore, at the implementation level, we choose $\delta t = \gamma \Delta t$, where $0 < \gamma \ll 1$ and Δt is the time-step discretization size, which will be introduced later in the work.A typical choice is $0 < \gamma \leqslant 0.01$. Typically, the system is insensitive to γ below 0.01. We assume $\delta t_1 + \delta t_2 = \delta t_1 + e\delta t_1$, which immediately allows the following definitions

$$\delta t_1 = \frac{\gamma \Delta t}{1+e} \quad \text{and} \quad \delta t_2 = \frac{e\gamma \Delta t}{1+e}. \tag{3.18}$$

These results are consistent with the fact that the recovery time vanishes (all compression and no recovery) for $e \to 0$ (asymptotically "plastic") and, as $e \to 1$, the recovery time equals the compression time ($\delta t_2 = \delta t_1$, asymptotically "elastic"). If $e = 1$, there is no loss in energy, while if $e = 0$ there is a maximum loss in energy. For a more detailed analysis of impact duration times, see Johnson [25].

Remark 2. It is obvious that for a deeper understanding of the deformation within a particle, it must be treated as a deformable continuum, which will require a spatial discretization, for example using the Finite Element Method of the body (particle). For work specifically focusing on the continuum mechanics of particles, see Zohdi and Wriggers [54]. For a detailed numerical analysis of multifield contact between bodies see Wriggers [45].

3.2. "Friction" (resistance to sliding)

To incorporate frictional[3] stick–slip phenomena during impact for a general particle pair (i and j), the tangential velocities at the beginning of the impact time interval (time = t) are computed by subtracting the relative normal velocity away from the total relative velocity:

$$\boldsymbol{v}_{jt}(t) - \boldsymbol{v}_{it}(t) = (\boldsymbol{v}_j(t) - \boldsymbol{v}_i(t)) - \big((\boldsymbol{v}_j(t) - \boldsymbol{v}_i(t)) \cdot \boldsymbol{n}_{ij}\big)\boldsymbol{n}_{ij}. \tag{3.19}$$

One then writes the equation for tangential momentum change during impact for the *ith* particle

$$m_i v_{it}(t) - \bar{I}_f \delta t + \overline{\mathcal{E}}_{it}\delta t = m_i v_{ct}, \tag{3.20}$$

where the friction contribution is

$$\bar{I}_f = \frac{1}{\delta t}\int_t^{t+\delta t} I_f\, dt, \tag{3.21}$$

where the total contributions from all other particles in the tangential direction ($\boldsymbol{\tau}_{ij}$) are

$$\overline{\mathcal{E}}_{it} = \frac{1}{\delta t}\int_t^{t+\delta t} \mathcal{E}_i \cdot \boldsymbol{\tau}_{ij}\, dt \tag{3.22}$$

and where v_{ct} is the common velocity of particles i and j in the tangential direction.[4] Similarly, for the *jth* particle we have

$$m_j v_{jt}(t) + \bar{I}_f \delta t + \overline{\mathcal{E}}_{jt}\delta t = m_j v_{ct}. \tag{3.23}$$

[3] It is probably more accurate to refer to this as "resistance to sliding" at such small scales, however, for brevity, we refer to the effect as "friction".

[4] They do not move relative to one another.

There are two unknowns, $\bar{I}_f$ and v_{ct}. The main quantity of interest is $\bar{I}_f$, which can be solved for

$$\bar{I}_f = \frac{\left(\frac{\bar{\varepsilon}_{it}}{m_i} - \frac{\bar{\varepsilon}_{jt}}{m_j}\right)\delta t + v_{it}(t) - v_{jt}(t)}{\left(\frac{1}{m_i} + \frac{1}{m_j}\right)\delta t}. \tag{3.24}$$

Thus, consistent with stick–slip models of Coloumb friction, one first assumes no slip occurs. If

$$|\bar{I}_f| > \mu_s |\bar{I}_n|, \tag{3.25}$$

where

$$\mu_s \geqslant \mu_d \tag{3.26}$$

is the coefficient of *static* friction, then slip must occur and a dynamic sliding friction model is used. If sliding occurs, the friction force is assumed to be proportional to the normal force and opposite to the direction of relative tangent motion, i.e.

$$\boldsymbol{\Psi}_i^{fric} \stackrel{\text{def}}{=} \mu_d ||\boldsymbol{\Psi}^{con}|| \frac{\boldsymbol{v}_{jt} - \boldsymbol{v}_{it}}{||\boldsymbol{v}_{jt} - \boldsymbol{v}_{it}||} = -\boldsymbol{\Psi}_j^{fric}. \tag{3.27}$$

3.3. Velocity-dependent coefficients of restitution

It is important to realize that, in reality, the phenomenological parameter e depends on the severity of the impact velocity. For extensive experimental data, see Goldsmith [19], or Johnson [25] for a more detailed analytical treatment. A mathematical idealization of the behavior can be constructed as follows

$$e \stackrel{\text{def}}{=} max\left(e_o\left(1 - \frac{\Delta v_n}{v^*}\right), e^-\right). \tag{3.28}$$

where v^* is a critical threshold velocity (normalization) parameter and where the relative velocity of approach is defined by

$$\Delta v_n \stackrel{\text{def}}{=} |v_{jn}(t) - v_{in}(t)| \tag{3.29}$$

and e^- is a lower limit to the coefficient of restitution.

Remarks. Later, we will consider examples where particles impact a wall (substrate). The impact forces between a particle and wall are handled in a similar manner as a particle-to-particle impact, except with no near-field interaction. The wall is assumed to be always stationary (with infinite mass), in the previous expressions derived for particle-to-particle impact.[5] Also, to insure that there is no interpenetration of the particle into the wall, a repulsive "restoring" (penalty) force term of the form

$$\boldsymbol{\Psi}_i^{wall} = K||\boldsymbol{r}_i - \boldsymbol{r}_{wall}||^{\beta} \boldsymbol{n}_{iw} \tag{3.30}$$

is activated if there is particle penetration into the wall ($\boldsymbol{n}_{iw}$ is the normal direction to the wall surface). K is a large positive penalty term and $1 < \beta$. The model can be interpreted as a (contact) penalty for particle–wall interpenetration. We also note that in many applications the near-fields can dramatically change when the particles are very close to one another, leading to increased repulsion (for example, due to repulsive interpenetration forces) or attraction (for example, due to adhesion). A particularly straightforward way to model this is via a near-field attractive/repulsive *augmentation* of the form

$$\tilde{\boldsymbol{\Psi}}_i^{nf} = \boldsymbol{\Psi}_i^{nf} + \underbrace{\alpha_a ||\boldsymbol{r}_i - \boldsymbol{r}_j||^{\beta_a} \boldsymbol{n}_{ij}}_{\boldsymbol{\Psi}^a \stackrel{\text{def}}{=} \text{augmentation force}}, \tag{3.31}$$

which is activated if

$$||\boldsymbol{r}_i - \boldsymbol{r}_j|| \leqslant (r_{pi} + r_{pj})\delta_a, \tag{3.32}$$

where r_{pi} and r_{pj} are the radii of the particles, and where $\delta_a \geqslant 0$ is the critical distance needed for the augmentation to become active. When $\delta_a = 1$ and $\alpha_a < 0$, then the model can be interpreted as a (contact) penalty for particle interpenetration. Many such "augmentation" models exist. For a lengthy discussion of interpenetration models see, for example, Duran [14]. For many engineering materials, some surface adhesion persists, which can lead to bonding phenomena between surfaces, even when no explicit external charging has occurred. For example, see Tabor [40] and Rietema [37] (specifically for agglomeration). We have not included these augmentation forces in the near-field models in this paper.

[5] The wall surface will be assumed to possess an electric field, thus already taking into account near-field effects.

4. Decomposed time-stepping and adaptive recursion

For the considered class of problems, it is advantageous to follow a "collide and stream" philosophy, similar to Lattice–Boltzmann methods,[6] whereby collisions are evaluated at the beginning of the time-step (i.e. $t^* = t$, updated at the end of the previous time-step). This also mitigates large numbers operations associated with continuous contact searches within time-steps. This is discussed in more depth at the end of this section.

4.1. A hybrid (split) time-stepping scheme for impact

Separating the impulsive and continuous forces in Eq. 2.1 leads to (a modification of the midpoint rule with $0 \leqslant \phi \leqslant 1$, see Appendix)

$$\begin{aligned}\boldsymbol{v}_i(t+\Delta t) &= \boldsymbol{v}_i(t) + \frac{1}{m_i}\int_t^{t+\Delta t} \boldsymbol{\Psi}_i^{tot}\, dt = \boldsymbol{v}_i(t) + \frac{1}{m_i}\left(\int_t^{t+\Delta t} (\boldsymbol{\Psi}_i^{nf} + \boldsymbol{\Psi}_i^{env})\, dt + \int_t^{t+\delta t} \boldsymbol{\Psi}_i^{con}\, dt + \int_t^{t+\delta t} \boldsymbol{\Psi}_i^{fric}\, dt\right)\\ &\approx \boldsymbol{v}_i(t) + \frac{\Delta t}{m_i}\Big(\phi\Big(\boldsymbol{\Psi}_i^{nf}(t+\Delta t) + \boldsymbol{\Psi}_i^{env}(t+\Delta t)\Big) + (1-\phi)\Big(\boldsymbol{\Psi}_i^{nf}(t) + \boldsymbol{\Psi}_i^{env}(t)\Big)\Big) + \frac{\delta t}{m_i}\Big(\overline{\boldsymbol{\Psi}}_i^{con}(t^*) + \overline{\boldsymbol{\Psi}}_i^{fric}(t^*)\Big), \end{aligned} \tag{4.1}$$

where $t \leqslant t^* \leqslant t + \Delta t$, is a moment in time where the contact is evaluated (this is discussed in more depth shortly). The position can be computed via

$$\begin{aligned}\boldsymbol{r}_i(t+\Delta t) = \boldsymbol{r}_i(t) + \boldsymbol{v}_i(t)\Delta t + \frac{\phi(\Delta t)^2}{m_i}\Big(\phi\Big(\boldsymbol{\Psi}_i^{nf}(t+\Delta t) + \boldsymbol{\Psi}_i^{env}(t+\Delta t)\Big) + (1-\phi)\Big(\boldsymbol{\Psi}_i^{nf}(t) + \boldsymbol{\Psi}_i^{env}(t)\Big)\Big)\\ + \frac{\phi\Delta t\delta t}{m_i}\Big(\overline{\boldsymbol{\Psi}}_i^{con}(t^*) + \overline{\boldsymbol{\Psi}}_i^{fric}(t^*)\Big). \end{aligned} \tag{4.2}$$

Remarks. Generally speaking, if a recursive process is *not employed* (an explicit scheme), the iterative error can accumulate rapidly. However, an overkill approach involving very small time steps, smaller than needed to control the discretization error, simply to suppress a nonrecursive process error, is computationally inefficient. This is discussed next.

4.2. Iterative (implicit) solution method

We now develop an adaptive iterative scheme by building on an approach found in various forms in Zohdi [46–54]. We write Eq. 4.2 in a slightly more streamlined form for particle i (superscript L is a time interval counter)

$$\boldsymbol{r}_i^{L+1} = \boldsymbol{r}_i^L + \boldsymbol{v}_i^L\Delta t + \frac{\phi(\Delta t)^2}{m_i}\Big(\phi\Big(\boldsymbol{\Psi}_i^{nf,L+1} + \boldsymbol{\Psi}_i^{env,L+1}\Big) + (1-\phi)\Big(\boldsymbol{\Psi}_i^{nf,L} + \boldsymbol{\Psi}_i^{env,L}\Big)\Big) + \frac{\phi\Delta t\delta t}{m_i}\Big(\overline{\boldsymbol{\Psi}}_i^{con}(t^*) + \overline{\boldsymbol{\Psi}}_i^{fric}(t^*)\Big), \tag{4.3}$$

which leads to a coupled set equations for $i = 1, 2 \ldots N_p$ particles.

The set of equations represented by Eq. (4.3) can be solved recursively. Eq. (4.3) can be solved recursively by recasting the relation as (provided we follow the collide and stream philosophy and select $t^* = t$)

$$\boldsymbol{r}_i^{L+1,K} = \underbrace{\boldsymbol{r}_i^L + \boldsymbol{v}_i^L\Delta t + \frac{\phi(1-\phi)(\Delta t)^2}{m_i}\Big(\boldsymbol{\Psi}_i^{nf,L} + \boldsymbol{\Psi}_i^{env,L}\Big) + \frac{\phi\Delta t\delta t}{m_i}\Big(\overline{\boldsymbol{\Psi}}_i^{con,L} + \overline{\boldsymbol{\Psi}}_i^{fric,L}\Big)}_{\mathcal{R}} + \underbrace{\frac{(\phi\Delta t)^2}{m_i}\Big(\boldsymbol{\Psi}_i^{nf,L+1,K-1} + \boldsymbol{\Psi}_i^{env,L+1,K-1}\Big)}_{\mathcal{G}(\boldsymbol{r}_i^{L+1,K-1})}, \tag{4.4}$$

where we define

$$\boldsymbol{\Psi}_i^{nf\ or\ env,L} \stackrel{\text{def}}{=} \boldsymbol{\Psi}_i^{nf\ or\ env,L}(\boldsymbol{r}_1^L, \boldsymbol{r}_2^L \ldots \boldsymbol{r}_N^L) \tag{4.5}$$

and

$$\boldsymbol{\Psi}_i^{nf\ or\ env,L+1,K-1} \stackrel{\text{def}}{=} \boldsymbol{\Psi}_i^{nf\ or\ env,L+1,K-1}(\boldsymbol{r}_1^{L+1,K-1}, \boldsymbol{r}_2^{L+1,K-1} \ldots \boldsymbol{r}_N^{L+1,K-1}). \tag{4.6}$$

Eq. (4.4) is of the form

$$\boldsymbol{r}_i^{L+1,K} = \mathcal{G}(\boldsymbol{r}_i^{L+1,K-1}) + \mathcal{R}_i, \tag{4.7}$$

where $K = 1, 2, 3, \ldots$ is the index of iteration within time step $L+1$ and $\mathcal{R}_i$ is a remainder term that does not depend on the solution at $L+1$. The convergence of such a scheme is dependent on the behavior of $\mathcal{G}$. Namely, a sufficient condition for convergence is that $\mathcal{G}$ is a contraction mapping for all $\boldsymbol{r}_i^{L+1,K}$, $K = 1, 2, 3 \ldots$ In order to investigate this further, we define the iteration error as

[6] See, for example, Sukop and Thorne [40] for a basic introduction to Lattice–Boltzmann methods.

$$\varpi_i^{L+1,K} \stackrel{\text{def}}{=} \boldsymbol{r}_i^{L+1,K} - \boldsymbol{r}_i^{L+1}. \tag{4.8}$$

A necessary restriction for convergence is iterative self consistency, i.e. the "exact" (discretized) solution must be represented by the scheme, $\boldsymbol{r}_i^{L+1} = \mathcal{G}(\boldsymbol{r}_i^{L+1}) + \mathcal{R}_i$. Enforcing this restriction, a sufficient condition for convergence is the existence of a contraction mapping

$$\| \underbrace{\boldsymbol{r}_i^{L+1,K} - \boldsymbol{r}_i^{L+1}}_{\varpi_i^{L+1,K}} \| = ||\mathcal{G}(\boldsymbol{r}_i^{L+1,K-1}) - \mathcal{G}(\boldsymbol{r}_i^{L+1})|| \leqslant \eta^{L+1,K} ||\boldsymbol{r}_i^{L+1,K-1} - \boldsymbol{r}_i^{L+1}||, \tag{4.9}$$

where, if $0 \leqslant \eta^{L+1,K} < 1$ for each iteration K, then $\varpi_i^{L+1,K} \rightarrow \boldsymbol{0}$ for any arbitrary starting value $\boldsymbol{r}_i^{L+1,K=0}$, as $K \rightarrow \infty$, which is a contraction condition that is sufficient, but not necessary, for convergence. The convergence of Eq. 4.4 is dictated by the operator $\mathcal{G}$, which in turn is scaled by η, which has the following proportionality:

$$\eta \propto \frac{(\phi \Delta t)^2}{m_i} \left(||\boldsymbol{\Psi}_i^{nf}|| + ||\boldsymbol{\Psi}_i^{env}|| \right). \tag{4.10}$$

Therefore, we see that the contraction constant of $\mathcal{G}$ is (1) directly dependent on the strength of the interaction forces, (2) inversely proportional to m_i and (3) directly proportional to $(\Delta t)^2$ (at time = t). Thus, decreasing the time step size improves the convergence. *In order to simultaneously maximize the time-step sizes to decrease overall computing time, while still meeting an error tolerance on the numerical solution's accuracy*, we build on an approach found in Zohdi [46] originally developed for continuum thermo-chemical multifield problems, in which one approximates $\eta^{L+1,K} \approx S(\Delta t)^p$, ($S$ is assumed a constant at that iteration) and one assumes that the error within an iteration to behave according to

$$(S(\Delta t)^p)^K \varpi^{L+1,0} = \varpi^{L+1,K}, \tag{4.11}$$

$K = 1, 2, \ldots$, where $\varpi^{L+1,0} = ||\boldsymbol{r}^{L+1,K=1} - \boldsymbol{r}^L||$ is the initial norm of the iterative (relative) error and S is intrinsic to the system, where, for example, for the class of problems under consideration, due to the quadratic dependency on Δt, $p \approx 2$. Our goal is to meet an error tolerance in exactly a preset (the analyst sets this) number of iterations. To this end, one writes

$$(S(\Delta t_{\text{tol}})^p)^{K_d} \varpi^{L+1,0} = TOL, \tag{4.12}$$

where TOL is a tolerance and where K_d is the number of desired iterations. If the error tolerance is not met in the desired number of iterations, the contraction constant $\eta^{L+1,K}$ is too large. Accordingly, one can solve (solving Eqs. 4.11 and 4.12 simultaneously) for a new smaller step size

$$\Delta t_{\text{tol}} = \Delta t \left(\frac{(\frac{TOL}{\varpi^{L+1,0}})^{\frac{1}{pK_d}}}{(\frac{\varpi^{L+1,K}}{\varpi^{L+1,0}})^{\frac{1}{pK}}} \right). \tag{4.13}$$

Notice that S scales out of Eq. 4.13. The assumption that S is constant is not critical, since the time steps are to be recursively refined and unrefined throughout the simulation. Once the relative positions of the particles have stabilized within a time step, S stabilizes and is constant. Clearly, the expression in Eq. 4.13 can also be used for time step enlargement, if convergence is met in less than a desired set of iterations, denoted K_d (typically chosen to be between five to ten iterations).

Remarks: In order to further illustrate the type of fixed point iterations adopted in this work, consider a simple implicit discretization (for illustration purposes only) of an isolated particle:

$$m\ddot{r} \approx \frac{r(t+\Delta t) - 2r(t) + r(t-\Delta t)}{(\Delta t)^2} = \Psi(r(t+\Delta t)), \tag{4.14}$$

which yields, using the shorthand superscript notation for time-stepping

$$r^{L+1} = 2r^L - r^{L-1} + \frac{(\Delta t)^2}{m} \Psi^{L+1}, \tag{4.15}$$

which has the form described in the body of the paper and motivates the expression cited in the text: $\eta^{L+1,K} \approx S(\Delta t)^p$, with $p = 2$. Depending on the nature of Ψ^{L+1}, which depends on r^{L+1}, S will change. This approach (assuming $\eta^{L+1,K} \approx S(\Delta t)^p$) is essentially a Secant-type method, as opposed to a Newton-type scheme, which would attempt to linearize Ψ^{L+1}. Newton's method does, in theory, however help characterize S, via a linearization of the righthand side of the term Ψ^{L+1} in Eq. (4.15) (with iterations $K = 1, 2, \ldots$)

$$r^{L+1,K} \approx 2r^L - r^{L-1} + \frac{(\Delta t)^2}{m} \left(\Psi^{L+1,K-1} + \left. \frac{\partial \Psi}{\partial r} \right|_{r^{L+1,K}} \right). \tag{4.16}$$

In this case, one can immediately identify $S = \frac{(\Delta t)^2}{m} \frac{\partial \Psi}{\partial r}|_{r^{L+1,K}}$. Such a linearization would be extraordinarily difficult to do for a multifield-multibody system undergoing collisions (since Ψ will be unsmooth and nonconvex). Specifically, to illustrate the difficulties with applying Newton's method to this class of problems consider the residual defined by the system represented in abstract form

$$\mathbf{\Pi} \stackrel{\text{def}}{=} \mathcal{A}(\boldsymbol{r}) - \mathcal{F}. \tag{4.17}$$

Linearization leads to

$$\mathbf{\Pi}(\boldsymbol{r}^K) = \mathbf{\Pi}(\boldsymbol{r}^{K-1}) + \nabla_{\boldsymbol{r}}\mathbf{\Pi}|_{\boldsymbol{r}^{K-1}}(\boldsymbol{r}^K - \boldsymbol{r}^{K-1}) + \mathcal{O}(||\boldsymbol{r}^K - \boldsymbol{r}^{K-1}||^2), \tag{4.18}$$

and thus the Newton updating scheme can be developed by enforcing,

$$\mathbf{\Pi}(\boldsymbol{r}^K) \approx \mathbf{0}, \tag{4.19}$$

leading to

$$\boldsymbol{r}^K = \boldsymbol{r}^{K-1} - (\mathcal{A}^{TAN,K-1})^{-1}\mathbf{\Pi}(\boldsymbol{r}^{K-1}), \tag{4.20}$$

where

$$\mathcal{A}^{TAN,K} = (\nabla_{\boldsymbol{r}}\mathcal{A}(\boldsymbol{r}))|_{\boldsymbol{r}^K} = (\nabla_{\boldsymbol{r}}\mathbf{\Pi}(\boldsymbol{r}))|_{\boldsymbol{r}^K}, \tag{4.21}$$

is the tangent. Therefore, in the fixed-point form one has the operator

$$\mathcal{G}(\boldsymbol{r}) = \boldsymbol{r} - (\mathcal{A}^{TAN})^{-1}\mathbf{\Pi}(\boldsymbol{r}). \tag{4.22}$$

For the problems considered, involving contact, friction, near-field forces, etc., it is unlikely that the tangents of $\mathcal{A}$ remain positive definite, or even that $\mathcal{A}$ is continuously differentiable, due to the impact events. Essentially, $\mathcal{A}$ will have nonconvex and nondifferentiable dependence on the positions of the particles. Thus, a fundamental difficulty is the possibility of a zero or nonexistent tangent ($\mathcal{A}^{TAN}$). Therefore, while Newton's method usually converges at a faster rate than a direct fixed point iteration, quadratic as opposed to superlinear, *its range of applicability is less robust.* The approach adopted in this paper approximates the tangent by a Secant, and thus does experience the difficulties with nondifferentiability of tangents or their loss of positive-definiteness. Early papers of the author have discussed the difficulties with such a linearization at length. For example,see Zohdi [52].

4.3. Algorithm/solution steps

Specifically, for the multibody system, the algorithm within solution steps are, within a time-step:

- (1): Start a global fixed iteration (set $i = 1$ and $K = 1$)
- (2): If $i > N_p$ then go to (4)
- (3): If $i \leqslant N_p$ then:
  (a) Compute the position $\boldsymbol{r}_i^{L+1,K}$
  (b) Go to (2) for the next particle ($i = i + 1$)
- (4): Measure error (normalized) quantities
  (a) $\varpi^K \stackrel{\text{def}}{=} \frac{\sum_{i=1}^{N_p} ||\boldsymbol{r}_i^{L+1,K} - \boldsymbol{r}_i^{L+1,K-1}||}{\sum_{i=1}^{N_p} ||\boldsymbol{r}_i^{L+1,K} - \boldsymbol{r}_i^{L}||}$
  (b) $Z^K \stackrel{\text{def}}{=} \frac{\varpi^K}{TOL}$
  (c) $\Phi^K \stackrel{\text{def}}{=} \left(\frac{\left(\frac{TOL}{\varpi^0}\right)^{\frac{1}{pK_d}}}{\left(\frac{\varpi^K}{\varpi^0}\right)^{\frac{1}{pK}}} \right)$
- (5): If the tolerance is met: ($Z^K \leqslant 1$) and $K < K_d$ then
  (a) Increment time: $t = t + \Delta t$
(b) Construct the next time step: $(\Delta t)^{new} = \Phi^K(\Delta t)^{old}$,
(c) Select the minimum size: $\Delta t = MIN((\Delta t)^{lim}, (\Delta t)^{new})$ and go to (1)
- (6): If the tolerance is not met: ($Z^K > 1$) and $K < K_d$ then
  (a) Update the iteration: $K = K + 1$
(b) Reset the particle counter: $i = 1$
(c) Go to (2)
- (7): If the tolerance is not met ($Z^K > 1$) and $K = K_d$ then
  (a) Construct a new time step: $\Delta t = \Phi^K \Delta t$
  (b) Restart at time t and go to (1)

Time-step size adaptivity is critical, since the system's dynamics and configuration can dramatically change over the course of time, possibly requiring quite different time step sizes to control the iterative error. However, to maintain the accuracy of the time-stepping scheme, one must respect an upper bound dictated by the discretization error, i.e., $\Delta t \leqslant (\Delta t)^{lim}$. Note that in step (5), Φ^K may enlarge the time-step if the error is lower than the preset tolerance.

Remarks. An alternative approach to collide and stream paradigm is to select $0 < t^* \leqslant t + \Delta t$ (continuous contact search within the time interval, which is rather computationally expensive), which modifies Eq. 4.4 to become

$$\boldsymbol{r}_i^{L+1,K} = \underbrace{\boldsymbol{r}_i^L + \boldsymbol{v}_i^L \Delta t + \frac{\phi(1-\phi)(\Delta t)^2}{m_i}\left(\boldsymbol{\Psi}_i^{nf,L} + \boldsymbol{\Psi}_i^{env,L}\right)}_{\mathcal{R}} + \underbrace{\frac{(\phi \Delta t)^2}{m_i}\left(\boldsymbol{\Psi}_i^{nf,L+1,K-1} + \boldsymbol{\Psi}_i^{env,L+1,K-1}\right) + \frac{\phi \Delta t \delta t}{m_i}\left(\overline{\boldsymbol{\Psi}}_i^{con,L+1,K-1} + \overline{\boldsymbol{\Psi}}_i^{fric,L+1,K-1}\right)}_{\mathcal{G}(\boldsymbol{r}_i^{L+1,K-1})}. \tag{4.23}$$

The essential difference is that the contact would have to be checked during the time-interval calculations. In the absence of collisions, the time-stepping approach is second-order accurate (see the Appendix), if the choice of the time-stepping parameter in the trapezoidal rule is chosen to be $\phi = 0.5$ (the mid-point rule). As indicated, the choice of $t < t^* \leqslant t + \Delta t$ leads to checking for contact *continuously* during the implicit iterations during a time-step. This would be extraordinarily time-consuming. However, intuitively, choosing $t^* = t$ leads to a loss of one-order of accuracy since one does not check over a time-interval Δt, making it first order accurate. Because this type of system combines differential equations with algebraic equations, it falls squarely in the realm of Differential Algebraic Equation (DAE) systems. A formal proof of the exact order of error when multiple collisions take place within a time interval is well-outside the scope of this paper, and we refer to the seminal texts of Hairer et al. [21,22], which discuss these issues in depth. For the rest of the paper, we use the collide and stream approach (choosing $t^* = t$). We note that because the time-steps are quite small, the difference between choosing $t^* = t$ or $t < t^* \leqslant t + \Delta t$ to the overall result appears to be a genuinely minor issue, although the choice of $t < t^* \leqslant t + \Delta t$ is somewhat slower computationally, due to the repeated contact checks. Both approaches were investigated, for the class of problems of interest, with virtually no difference in the overall response of the systems tested later in the presentation, primarily because of the small time scales.

5. Numerical examples: impact on progressively electrified surfaces

5.1. Figures of merit for coating quality

Referring to Fig. 2, we consider the following logical figures of merit to assess the deposition process: (using an x–y–z triad with target center at $y = 0,\ z = 0$)

- Percent deposition within a target (radial) distance: summing the particles that satisfy $\sqrt{y_i^2 + z_i^2} \leqslant d^{tar}$, and dividing that number by the total number of particles N.
- Layer thickness, provided by: $\bar{x} = \frac{1}{N_p}\sum x_i$,
- Standard deviation from the mean layer thickness: $S(x_i - \bar{x}) = \frac{1}{N_p}\sum (x_i - \bar{x})^2$,
- Mean distance from the target center: $\bar{d} = \frac{1}{N_p}\sqrt{y_i^2 + z_i^2} \leqslant R^{tar}$
- Standard deviation from the mean distance: $S(d_i - \bar{d}) = \frac{1}{N_p}\sum (d_i - \bar{d})^2$,

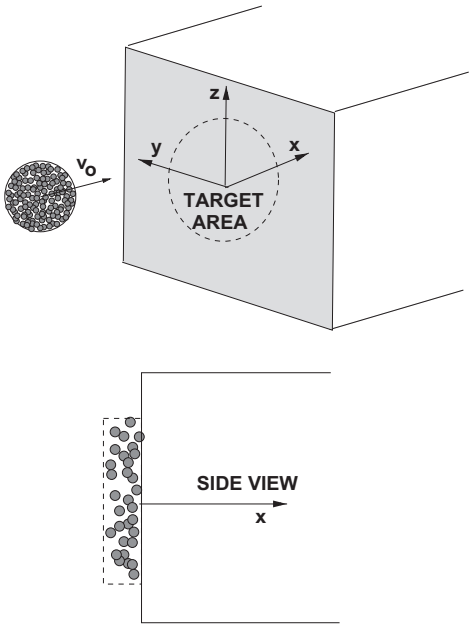

Fig. 2. Motivation for the figures of merit: desired uniform, flat deposition within a target zone.

5.2. System parameters

As an example, we considered a group of $N_p = 1000$ randomly positioned, non-overlapping, particles in a cluster-droplet domain (Fig. 3). The initial particle radius (monodisperse) was $r_p = 0.05$ m. The absolute dimensions are unimportant for the model problem, and have been normalized. The initial radius of the cluster-droplet was set to $R = 1$ initially. All system parameters can be scaled to describe any specific system of interest. The relevant simulation parameters were:

- number of particles = 1000,
- particle charges $q_i = 1,\ i = 1,\ldots,N_p$,
- $\alpha_{ij1} = 0.5,\ \alpha_{ij2} = 0.25,\ \beta_{ij1} = 1,\ \beta_{ij2} = 2$,
- mass density of the particles = 2000 kg/m^3,
- initial velocity = (50,0,0) m/s,
- initial mean position = (4,0,0) m,
- coefficient of dynamic friction, $\mu_d = 0.1$,
- coefficient of static friction, $\mu_s = 0.2$,
- baseline coefficient of restitution, $e_o = 0.5$,
- limit of coefficient of restitution, $e^- = 0.2$,
- velocity parameter, $v^* = 10$ m/s,
- target number of fixed point iterations, $K_d = 6$,
- the time-stepping parameter, $\phi = 0.5$,
- $\boldsymbol{E}^{ext} = (E_x^{ext}, 0, 0)$ Newtons/Coulomb, which starts after $x = 5$, with wall location at $x = 6$,

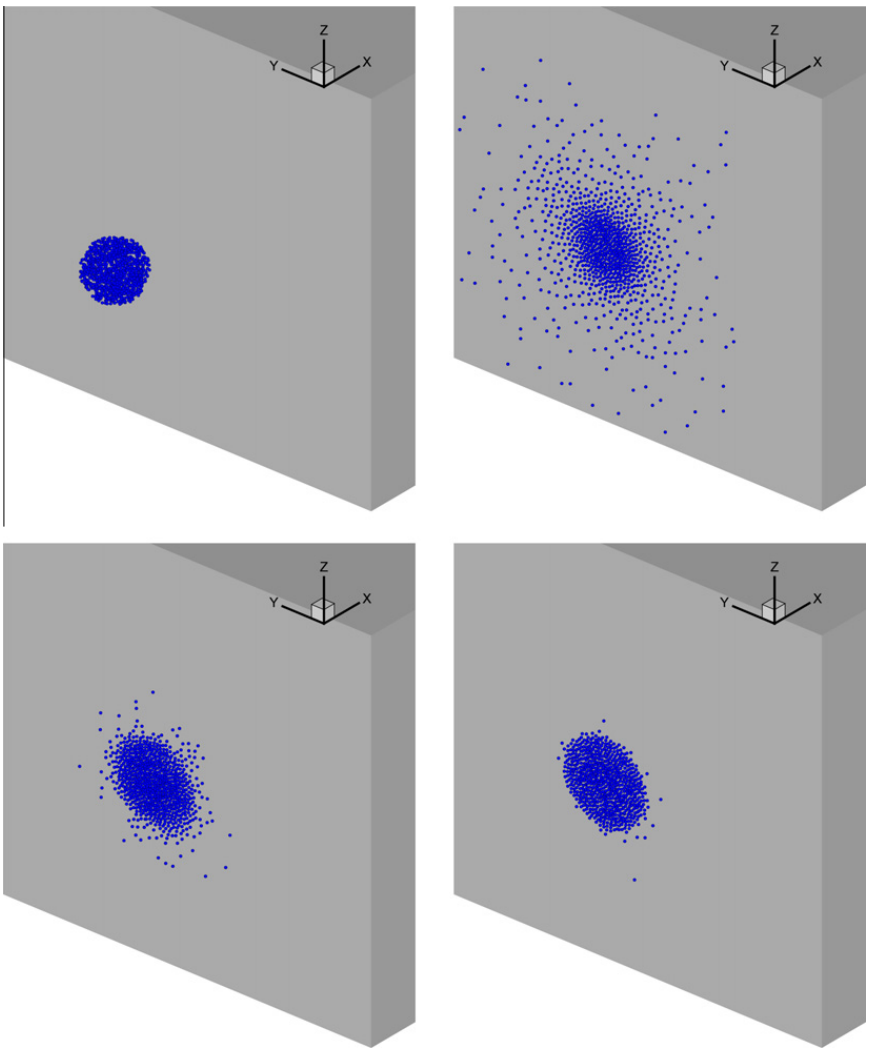

Fig. 3. Top Left: The starting configuration. Initially, the cluster-droplet's center is at $x = 4$, the electric field starts at $x = 5$ and the wall is at $x = 6$. The particles each have a radius of $r_p = 0.05$. Top right: the final configuration of a charged cluster-droplet for $E_x^{ext} = 100$ N/C, bottom left for $E_x^{ext} = 1000$ N/C and bottom right for $E_x^{ext} = 10,000$ N/C.

Table 1
The results as a function of increasing E-fields.

$E_x^{ext} - field$	$N_{p,in}/N_{p,tot}$	$\bar{d}$	$S(d_i - \bar{d})$	$\bar{x}$	$S(x_i - \bar{x})$
0.0	0.0630	5.4621	1.8121	4.1127	2.6920
1.0	0.0500	5.6404	1.7289	4.1851	2.7960
10.0	0.1120	5.1276	2.0841	5.5756	1.3868
100.0	0.6040	2.1860	1.7046	5.9498	0.0030
1000.0	0.9480	1.0680	0.5232	5.9500	0.0000
10000.0	0.9950	0.9898	0.4104	5.9504	0.0000

- simulation duration = 1 s,
- initial time step size = 0.001 s,
- time step upper bound = 0.0025 s,
- tolerance for the fixed-point iteration = 10^{-3}.

5.3. Results

Table 1 and Fig. 3 illustrate the trends with increasing electric fields. We have the following observations[7]:

- For the $E_x^{ext} - field \leqslant 1$ the particles rebound and do not adhere to the surface.
- For the $E_x^{ext} - field \approx 10$ the particles start to adhere with some limited rebounding (a behavior transition threshold),
- For the $E_x^{ext} - field \approx 100$ the particles adhere but spread over the surface incoherently,
- For the $E_x^{ext} - field \geqslant 1000$ the particles adhere and form a coherent "deposit", with their lateral motion dissipated by friction induced by the electric field contact force.

Remarks. To generate the initial particle configuration, the classical Random Sequential Addition (RSA) algorithm of Widom [44], which places nonoverlapping particles randomly into the domain of interest, while simultaneously checking for no particle overlaps, was used. However, we note that the RSA algorithm cannot achieve extremely high density (volume fraction) configurations. If high density packing of particles is needed, the well-known, equilibrium-driven, Metropolis algorithm can be used or, alternatively, another class of methods, based on simultaneous particle flow and growth developed in Kansaal et al. [26] and Donev et al. [9–13]. Such approaches have also been implemented for streams of particles in Zohdi [54].

5.4. Discussion: qualitative analysis of a single particle

In order to qualitatively understand the mechanisms that control the spreading of the droplet, let us consider a single isolated particle sliding on a surface (Fig. 4 on the left). One can determine the travel distance by equating the initial kinetic energy to the energy dissipated by sliding friction, where the normal force is supplied by the surface electric field (E) acting on the particle's charge q. This balance yields ($t = 0$ is the start and $t = T$ is the end)

$$\underbrace{\frac{1}{2} m v^2(0)}_{\text{initial kinetic energy}} = \underbrace{qE\mu_d x(T)}_{\text{energy dissipated}} \Rightarrow x(T) = \frac{m v^2(0)}{2qE\mu_d}. \tag{5.1}$$

We note that in order to determine the time-scale for this to occur, on can perform a momentum balance in the tangential direction, yielding

$$m v(0) - \int_0^T qE\mu_d \, dt = m v(T). \tag{5.2}$$

Setting $v(T) = 0$ gives $T = \frac{m v(0)}{qE\mu_d}$.

5.5. Analysis of two particles

Now let us repeat the analysis for two bound (charged) particles, with positions x_i and x_j, moving (sliding) in opposite directions (about the symmetry line in Fig. 4). For illustration purposes only, let us consider a linear attractive binding of $K(x_i - x_j)$, with binding stiffness $0 < K < \infty$, with corresponding energy $\frac{1}{2} K(x_i - x_j)^2$. Equating the stored, kinetic and dissipated energies, the point where the expansion stops (a maximum, relative to the symmetry line, where $v(T) = 0$) is denoted $x_i = -x_j = x(T)$ is (assuming a spring-like binding law with an unstretched separation (starting) state of $x_i - x_j = 2x(T)$)

[7] Particles that strayed outside of a computational 10 m × 10 m (y–z) window were thrown out of the computations.

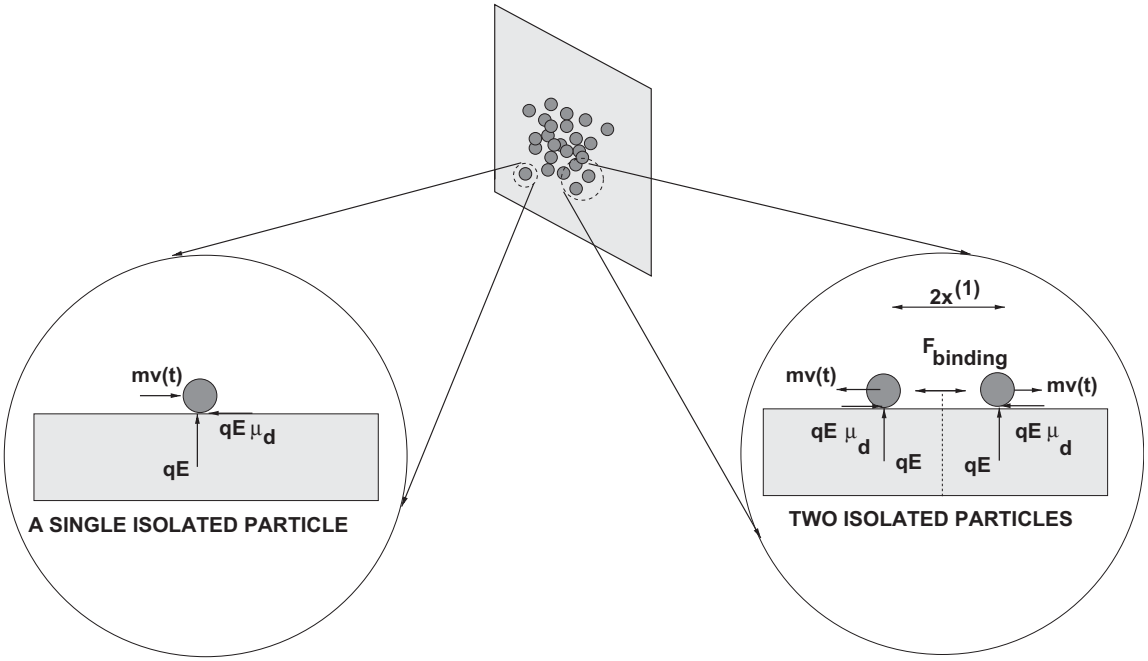

Fig. 4. Sliding with electrically-induced friction. Left: a single isolated particle. Right: two "bound" particles moving in opposite directions.

$$\frac{1}{2}K(2(x(T)-x(0)))^2 = 2\left(\frac{1}{2}mv^2(0) - qE\mu_d(x(T)-x(0))\right) = mv^2(0) - 2qE\mu_d(x(T)-x(0)). \tag{5.3}$$

Solving for $x(T)$ yields

$$x(T) = x(0) - \frac{qE\mu_d}{2K} \pm \left(\left(\frac{qE\mu_d}{2K}\right)^2 + \frac{mv(0)^2}{2K}\right)^{1/2}, \tag{5.4}$$

where the positive root is the physically-correct solution. We note the following trends

- as $qE\mu_d$ increases, $x(T)$ decreases,
- as K increases, $x(T)$ decreases and
- as $mv^2(0)$ increases, $x(T)$ increases.

Essentially, this qualitatively indicates how wide the cluster-droplet will spread.

Remarks. Clearly, $x(T)$ is the peak value of x, and the cluster-droplet may oscillate back and forth, until the friction dissipates all of the kinetic and stored energy. Any droplet retraction would likely be small in a real application, due to friction and interparticle collisions.

6. Conclusions

In summary, this work addressed the impact of charged cluster-droplets, comprised of particulates, on electrified surfaces, and developed numerical simulation techniques in order to investigate the post-impact structure of impacted cluster-droplets, which has wide-ranging applications in areas such as inkjet printing, sprays, coatings, etc. A numerical approach was developed whereby the dynamics of charged particles, accounting for their collisions, inter-particle near-fields, interaction with external electromagnetic fields are all computed implicitly in an iterative, modular, manner. A staggered, temporally-adaptive scheme was developed to resolve the drastic changes in the physical configuration of a cluster-droplet, for example when impacting an electrified wall/substrate. The approach developed provides a fast computational tool to analyze particulate cluster-droplets. Recently, the author has started a collaboration (see Choi et al. [3–5] and Demko et al. [8]) with an experimental team at UC Berkeley, and the use of the numerical tool to guide the experiments is currently underway The numerical approach and model can be used on virtually any type (shape) of cluster-droplet domain. Since the results are derived from a direct numerical simulation, one can also post-process other more detailed statistical information. For example, for any quantity of interest, Q (for example the positions of the particles, their velocities, etc.), with a distribution of values (Q_i, i = 1,2,...N_p = particles) about an arbitrary reference point, denoted $Q^\star$, as follows, via moments:

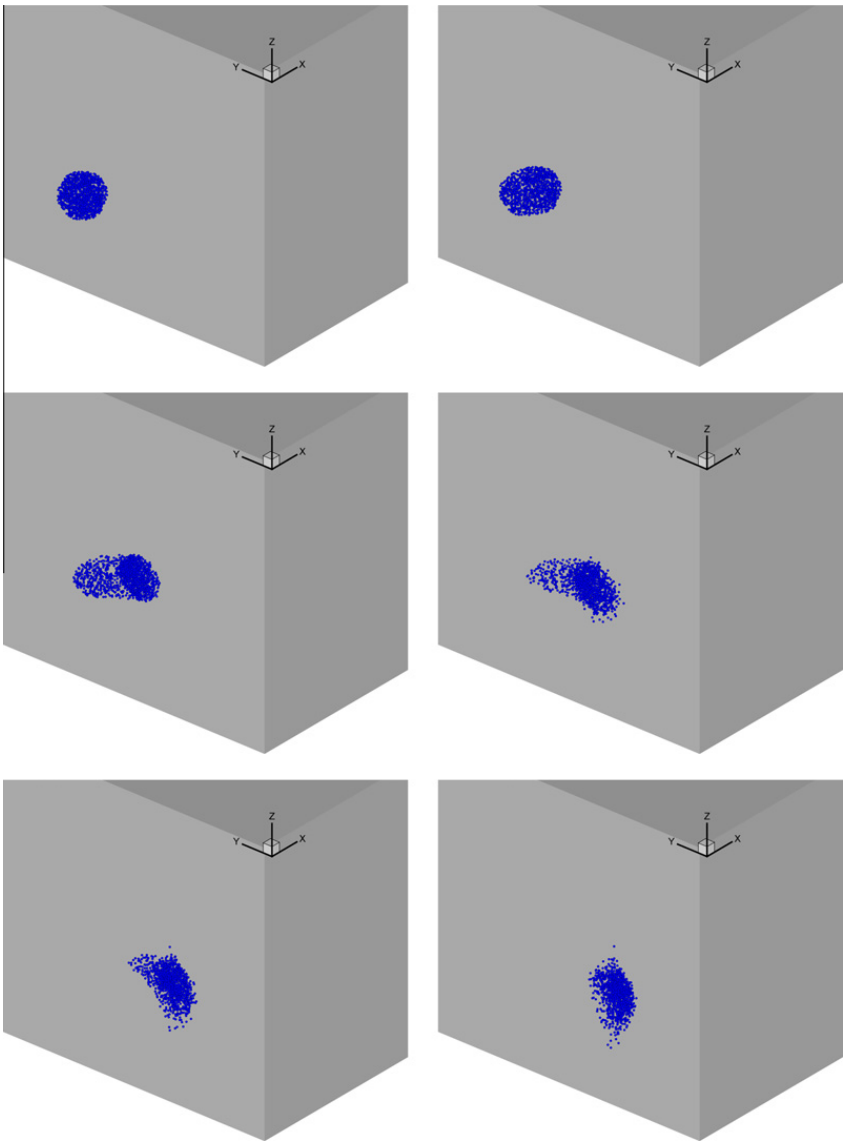

Fig. 5. Left to right and top to bottom: The bending of a droplet due to the presence of a magnetic field $\boldsymbol{B}^{ext} = (0, 100, 0)$ Ns/C m (also with $\boldsymbol{E}^{ext} = (10,000, 0, 0)$ N/C).

$$\boldsymbol{M}_r^{Q_i - Q^\star} \stackrel{\text{def}}{=} \frac{\sum_{i=1}^{N_p} a_i (Q_i - Q^\star)^r}{\sum_{i=1}^{N_p} a_i} \stackrel{\text{def}}{=} \overline{(Q_i - Q^\star)^r}. \tag{6.1}$$

Explicitly, the various moments characterize the distribution, for example:

1. $\boldsymbol{M}_1^{Q_i - A}$ measures the first deviation from the average, which equals zero,
2. $\boldsymbol{M}_1^{Q_i - 0} \stackrel{\text{def}}{=} \frac{\sum_{i=1}^{N_p} a_i (Q_i - 0)}{\sum_{i=1}^{N_p} a_i} \stackrel{\text{def}}{=} \overline{(Q_i - 0)} = A$,
3. $\boldsymbol{M}_2^{Q_i - A}$ is the standard deviation,
4. $\boldsymbol{M}_3^{Q_i - A}$ is the skewness, which measures the bias, or asymmetry of the distribution of data and
5. $\boldsymbol{M}_4^{Q_i - A}$ is the kurtosis (fourth moment), which measures the "tightness" of the distribution.[8]

This is straightforward to implement, and can provide much more detailed information on post-impact cluster-droplet characteristics.

Finally, in closing, some remarks on the effects of magnetic fields on a particulate cluster are appropriate. Magnetic fields, due to their production of Lorentz forces, $q_i \boldsymbol{v}_i \times \boldsymbol{B}^{ext}$, acting on each particle i will "bend" the overall trajectory of the entire

[8] For the purposes of this paper, the weight was $a_i = m_i$, although it could be different for other applications.

cluster-droplet, as shown in Fig. 5. Qualitative information can be extracted by initially studying a single isolated particle governed by

$$m\dot{\boldsymbol{v}}_i = q(\boldsymbol{E}^{ext} + \boldsymbol{v}_i \times \boldsymbol{B}^{ext}). \tag{6.2}$$

The governing equation 6.2 for component x is

$$\dot{v}_x = \frac{q}{m}(E_x^{ext} + (v_y B_z^{ext} - v_z B_y^{ext})), \tag{6.3}$$

for component y

$$\dot{v}_y = \frac{q}{m}(E_y^{ext} - (v_x B_z^{ext} - v_z B_x^{ext})), \tag{6.4}$$

and for component z

$$\dot{v}_z = \frac{q}{m}(E_z^{ext} + (v_x B_y^{ext} - v_y B_x^{ext})). \tag{6.5}$$

In the special case when $\boldsymbol{r}(t=0) = (r_{x0}, 0, 0)$, $\boldsymbol{v}(t=0) = (v_{x0}, 0, 0)$, $\boldsymbol{B}^{ext} = B_z^{ext}\boldsymbol{e}_z$ and $\boldsymbol{E}^{ext} = E_x^{ext}\boldsymbol{e}_x$, the solution for the trajectory of an isolated particle is

$$\left\{ \begin{array}{c} v_x(t) \\ v_y(t) \\ v_z(t) \end{array} \right\} = \left\{ \begin{array}{c} v_{x0}cos\omega t - \frac{q\omega E_x^{ext}}{m} sin\omega t \\ -v_{x0}sin\omega t - \frac{q\omega E_x^{ext}}{m} cos\omega t + \frac{q\omega E_x^{ext}}{m} \\ 0 \end{array} \right\} \tag{6.6}$$

and

$$\left\{ \begin{array}{c} r_x(t) \\ r_y(t) \\ r_z(t) \end{array} \right\} = \left\{ \begin{array}{c} \frac{1}{\omega}\left(v_{x0}sin\omega t + \frac{q\omega E_x^{ext}}{m} cos\omega t \right) - \frac{qE_x^{ext}}{m} + r_{x0} \\ \frac{1}{\omega}\left(v_{x0}cos\omega t - \frac{q\omega E_x^{ext}}{m} sin\omega t \right) + \frac{q\omega E_x^{ext} t}{m} - \frac{v_{x0}}{\omega} \\ 0 \end{array} \right\}. \tag{6.7}$$

where $\omega = \frac{qB_z^{ext}}{m}$ is known as the cyclotron frequency. The cyclotron frequency (gyrofrequency) is the angular frequency at which a charged particle makes circular orbits in a plane perpendicular to the static magnetic field. Notice that when $E_x^{ext} = 0$, this traces out the equation of a circle (in the x–y plane) centered at $(r_{x0}, -\frac{v_{x0}}{\omega}, 0)$. The radius of the "magnetically-induced circle" (radius of oscillation) is[9]

$$\mathcal{R} \stackrel{\text{def}}{=} \frac{v_{x0}}{\omega} = \frac{v_{x0} m}{q B_z^{ext}}. \tag{6.8}$$

Thus, if a desired "turning radius" is denoted by $\mathcal{R}$, one may solve for the magnetic field that delivers the desired effect, $B_z^{ext} = \frac{v_{x0} m}{q\mathcal{R}}$. The corresponding time period for one cycle to be completed is $T \stackrel{\text{def}}{=} 2\pi/\omega$. We note that since magnetic fields can bend flows, their use to coat complex parts by bending droplets around corners is possible. The influence of magnetic effects on the behavior of charged particulate clusters and the resulting deposition morphology are under investigation by the author.

Acknowledgments

The author thanks the Siemens Corporation and Dr. Ramesh Subramanian for partial financial support of this project.

Appendix A. Trapezoidal time-stepping schemes

Consider an equation of motion given by

$$m_i\dot{\boldsymbol{v}}_i = \boldsymbol{F}_i, \tag{8.1}$$

where $\boldsymbol{F}_i$ is the sum of (smooth) forces provided from interactions with the external environment. Expanding the velocity in a Taylor series about $t + \phi\Delta t$ we obtain

[9] This field generates helical-like motion in three dimensions when $\boldsymbol{E}_x^{ext} \neq \boldsymbol{0}$.

$$\boldsymbol{v}_i(t+\Delta t) = \boldsymbol{v}_i(t+\phi\Delta t) + \left.\frac{d\boldsymbol{v}_i}{dt}\right|_{t+\phi\Delta t}(1-\phi)\Delta t + \frac{1}{2}\left.\frac{d^2\boldsymbol{v}_i}{dt^2}\right|_{t+\phi\Delta t}(1-\phi)^2(\Delta t)^2 + \mathcal{O}(\Delta t)^3 \tag{8.2}$$

and

$$\boldsymbol{v}_i(t) = \boldsymbol{v}_i(t+\phi\Delta t) - \left.\frac{d\boldsymbol{v}_i}{dt}\right|_{t+\phi\Delta t}\phi\Delta t + \frac{1}{2}\left.\frac{d^2\boldsymbol{v}_i}{dt^2}\right|_{t+\phi\Delta t}\phi^2(\Delta t)^2 + \mathcal{O}(\Delta t)^3 \tag{8.3}$$

Subtracting the two expressions yields

$$\left.\frac{d\boldsymbol{v}_i}{dt}\right|_{t+\phi\Delta t} = \frac{\boldsymbol{v}_i(t+\Delta t) - \boldsymbol{v}_i(t)}{\Delta t} + \hat{\mathcal{O}}(\Delta t), \tag{8.4}$$

where $\hat{\mathcal{O}}(\Delta t) = \mathcal{O}(\Delta t)^2$, when $\phi = \frac{1}{2}$. Thus, inserting this into the equations of equilibrium yields

$$\boldsymbol{v}_i(t+\Delta t) = \boldsymbol{v}_i(t) + \frac{\Delta t}{m_i}\boldsymbol{F}_i(t+\phi\Delta t) + \hat{\mathcal{O}}(\Delta t)^2. \tag{8.5}$$

Note that adding a weighted sum of Eqs. 8.2 and 8.3 yields

$$\boldsymbol{v}_i(t+\phi\Delta t) = \phi\boldsymbol{v}_i(t+\Delta t) + (1-\phi)\boldsymbol{v}_i(t) + \mathcal{O}(\Delta t)^2, \tag{8.6}$$

which will be useful shortly. Now expanding the position of the center of mass in a Taylor series about $t+\phi\Delta t$ we obtain

$$\boldsymbol{r}_i(t+\Delta t) = \boldsymbol{r}_i(t+\phi\Delta t) + \left.\frac{d\boldsymbol{r}_i}{dt}\right|_{t+\phi\Delta t}(1-\phi)\Delta t + \frac{1}{2}\left.\frac{d^2\boldsymbol{r}}{dt^2}\right|_{t+\phi\Delta t}(1-\phi)^2(\Delta t)^2 + \mathcal{O}(\Delta t)^3 \tag{8.7}$$

and

$$\boldsymbol{r}_i(t) = \boldsymbol{r}_i(t+\phi\Delta t) - \left.\frac{d\boldsymbol{r}_i}{dt}\right|_{t+\phi\Delta t}\phi\Delta t + \frac{1}{2}\left.\frac{d^2\boldsymbol{r}_i}{dt^2}\right|_{t+\phi\Delta t}\phi^2(\Delta t)^2 + \mathcal{O}(\Delta t)^3. \tag{8.8}$$

Subtracting the two expressions yields

$$\frac{\boldsymbol{r}_i(t+\Delta t) - \boldsymbol{r}_i(t)}{\Delta t} = \boldsymbol{v}_i(t+\phi\Delta t) + \hat{\mathcal{O}}(\Delta t). \tag{8.9}$$

Inserting Eq. 8.6 yields

$$\boldsymbol{r}_i(t+\Delta t) = \boldsymbol{r}_i(t) + (\phi\boldsymbol{v}_i(t+\Delta t) + (1-\phi)\boldsymbol{v}_i(t))\Delta t + \hat{\mathcal{O}}(\Delta t)^2. \tag{8.10}$$

and thus using Eq. 8.5 yields

$$\boldsymbol{r}_i(t+\Delta t) = \boldsymbol{r}_i(t) + \boldsymbol{v}_i(t)\Delta t + \frac{\phi(\Delta t)^2}{m_i}\boldsymbol{F}_i(t+\phi\Delta t) + \hat{\mathcal{O}}(\Delta t)^2. \tag{8.11}$$

The term $\boldsymbol{F}_i(t+\phi\Delta t)$ can be handled in two main ways:

- $\boldsymbol{F}_i(t+\phi\Delta t) \approx \boldsymbol{F}_i(\phi\boldsymbol{r}_i(t+\Delta t) + (1-\phi)\boldsymbol{r}_i(t))$ or
- $\boldsymbol{F}_i(t+\phi\Delta t) \approx \phi\boldsymbol{F}_i(\boldsymbol{r}_i(t+\Delta t)) + (1-\phi)\boldsymbol{F}_i(\boldsymbol{r}_i(t))$.

The differences are quite minute between either of the above, thus, for brevity, we choose the latter. In summary, we have the following:

$$\boldsymbol{r}_i(t+\Delta t) = \boldsymbol{r}_i(t) + \boldsymbol{v}_i(t)\Delta t + \frac{\phi(\Delta t)^2}{m_i}(\phi\boldsymbol{F}_i(\boldsymbol{r}_i(t+\Delta t)) + (1-\phi)\boldsymbol{F}(\boldsymbol{r}_i(t))) + \hat{\mathcal{O}}(\Delta t)^2, \tag{8.12}$$

where

- when $\phi = 1$, then this is the (implicit) Backward Euler scheme, which is very stable (very dissipative) and $\hat{\mathcal{O}}(\Delta t)^2 = \mathcal{O}(\Delta t)^2$ locally in time,
- when $\phi = 0$, then this is the (explicit) Forward Euler scheme, which is conditionally stable and $\hat{\mathcal{O}}(\Delta t)^2 = \mathcal{O}(\Delta t)^2$ locally in time and
- when $\phi = 0.5$, then this is the (implicit) "Midpoint" scheme, which is stable and $\hat{\mathcal{O}}(\Delta t)^2 = \mathcal{O}(\Delta t)^3$ locally in time.

References

[1] D. Arbelaez, T.I. Zohdi, D. Dornfeld, Modeling and simulation of material removal with particulate flow, Computational Mechanics 42 (2008) 749–759.
[2] D. Arbelaez, T.I. Zohdi, D. Dornfeld, On impinging near-field granular jets, The International Journal of Numerical Methods in Engineering 80 (6) (2009) 815–845.
[3] S. Choi, I. Park, Z. Hao, H.Y. Holman, A.P. Pisano, T.I. Zohdi, Ultra-fast self-assembly of micro-scale particles by open channel flow, Langmuir 26 (7) (2010) 4661–4667.
[4] S. Choi, S. Stassi, A.P. Pisano, T.I. Zohdi, Coffee-ring effect-based three dimensional patterning of micro, nanoparticle assembly with a single droplet, Langmuir 26 (14) (2010) 11690–11698.
[5] S. Choi, A. Jamshidi, T.J. Seok, T.I. Zohdi, M.C. Wu, A.P. Pisano, Fast, high-throughput creation of size-tunable micro, nanoparticle clusters via evaporative self-assembly in picoliter-scale droplets of particle suspension, Langmuir 28 (6) (2012) 3102–3111.
[6] D. Ciampini, J.K. Spelt, M. Papini, Simulation of interference effects in particle streams following impact with a flat surface, Part I. Theory and Analysis. Wear 254 (2003) 237–249.
[7] D. Ciampini, J.K. Spelt, M. Papini, Simulation of interference effects in particle streams following impact with a flat surface. Part II. Parametric study and implications for erosion testing and blast cleaning, Wear 254 (2003) 250–264.
[8] M. Demko, S. Choi, T.I. Zohdi, A.P. Pisano, High resolution patterning of nanoparticles by evaporative self-assembly enabled by in-situ creation and mechanical lift-off of a polymer template, Applied Physics Letters 99 (2012) 253102-1–253102-3.
[9] A. Donev, I. Cisse, D. Sachs, E.A. Variano, F. Stillinger, R. Connelly, S. Torquato, P. Chaikin, Improving the density of jammed disordered packings using ellipsoids, Science 303 (2004) 990–993.
[10] A. Donev, F.H. Stillinger, P.M. Chaikin, S. Torquato, Unusually dense crystal ellipsoid packings, Physical Review Letters 92 (2004) 255506.
[11] A. Donev, S. Torquato, F. Stillinger, Neighbor list collision-driven molecular dynamics simulation for nonspherical hard particles-I. Algorithmic details, Journal of Computational Physics 202 (2005) 737.
[12] A. Donev, S. Torquato, F. Stillinger, Neighbor list collision-driven molecular dynamics simulation for nonspherical hard particles-II. Application to ellipses and ellipsoids, Journal of Computational Physics 202 (2005) 765.
[13] A. Donev, S. Torquato, F.H. Stillinger, Pair correlation function characteristics of nearly jammed disordered and ordered hard-sphere packings, Physical Review E 71 (2005) 011105.
[14] J. Duran, Sands, powders and grains, An Introduction to the Physics of Granular Matter, Springer-Verlag, 1997.
[15] M. Frenklach, C.S. Carmer, Molecular dynamics using combined quantum & empirical forces: application to surface reactions, Advances in Classical Trajectory Methods 4 (1999) 27–63.
[16] A. Ghobeity, J.K. Spelt, M. Papini, Abrasive jet micro-machining of planar areas and transitional slopes, Journal of Micromechanics and Microengineering 18 (2008) 055014.
[17] A. Ghobeity, T. Krajac, T. Burzynski, M. Papini, J.K. Spelt, Surface evolution models in abrasive jet micromachining, Wear 264 (2008) 185–198.
[18] S. Ghosh, D.M. Valiveti, S.H. Harris, J. Boileau, Microstructure characterization based domain partitioning as a pre-processor to multi-scale modeling of cast aluminum alloys, Modeling and Simulation in Materials Science and Engineering 14 (2006) 1363–1396.
[19] W. Goldsmith, Impact: The Theory & Physical Behavior of Colliding Solids, Dover Re-issue, Toronto, 2001.
[20] C. Gomes-Ferreira, D. Ciampini, M. Papini, The effect of inter-particle collisions in erosive streams on the distribution of energy flux incident to a flat surface, Tribology International 37 (2004) 791–807.
[21] E. Hairer, S.P. Norsett, G. Wanner, Solving Ordinary Differential Equations I. Nonstiff Equations, second ed., Springer-Verlag, 2000.
[22] E. Hairer, C. Lubich, G. Wanner, Solving Ordinary Differential Equations II. Stiff and Differential-Algebraic Problems, second ed., Springer-Verlag, 2006.
[23] W.L. Hase, Molecular Dynamics of Clusters, Surfaces, Liquids, & Interfaces, Advances in Classical Trajectory Methods, vol. 4, JAI Press, 1999.
[24] J.M. Haile, Molecular Dynamics Simulations: Elementary Methods, Wiley, 1992.
[25] K. Johnson, Contact Mechanics, Cambridge University Press, 1985.
[26] A. Kansaal, S. Torquato, F. Stillinger, Diversity of order and densities in jammed hard-particle packings, Physical Review E 66 (2002) 041109.
[27] L. Luo, D.A. Dornfeld, Material removal mechanism in chemical mechanical polishing: theory and modeling, IEEE Transaction: Semiconductor Manufacturing 14 (2) (2001) 112–133.
[28] L. Luo, D.A. Dornfeld, Effects of abrasive size distribution in chemical-mechanical planarization: modeling and verification, IEEE Transaction: Semiconductor Manufacturing 16 (2003) 469–476.
[29] L. Luo, D.A. Dornfeld, Material removal regions in chemical mechanical planarization for sub-micron integration for sub-micron integrated circuit fabrication: coupling effects of slurry chemicals, abrasive size distribution, and wafer-pad contact area, IEEE Transaction: Semiconductor Manufacturing 16 (2003) 45–56.
[30] L. Luo, D.A. Dornfeld, Integrated Modeling of Chemical Mechanical Planarization of Sub-micron IC Fabrication, Springer-Verlag, 2004.
[31] P. Martin, Handbook of Deposition Technologies for Films and Coatings, third ed., Elsevier, 2009.
[32] P. Martin, Introduction to Surface Engineering and Functionally Engineered Materials, Scrivener and Elsevier, 2011.
[33] E.A. Moelwyn-Hughes, Physical Chemistry, Pergamon, 1961.
[34] D.C. Rapaport, The Art of Molecular Dynamics Simulation, Cambridge University Press, 1995.
[35] M. Rechtsman, F.H. Stillinger, S. Torquato, Designed interaction potentials via inverse methods for self-assembly, Physical Review E 73 (2006) 011406.
[36] M. Rechtsman, F.H. Stillinger, S. Torquato, Optimized interactions for targeted self-assembly: application to honeycomb lattice, Physical Review Letters 95 (2005) 228301.
[37] K. Rietema, Dynamics of Fine Powders, Springer, 1991.
[38] F.H. Stillinger, T.A. Weber, Computer simulation of local order in condensed phases of silicon, Physisc Review B 31 (1985) 5262–5271.
[39] M.C. Sukop, D.T. Thorne, Lattice–Boltzmann Modeling: An Introduction for Geoscientists and Engineers, Springer-Verlag, 2006.
[40] D. Tabor, Interaction between surfaces: adhesion and friction, in: Blakely (Ed.), Surface Physics of Materials, vol. II, Academic Press, New York, San Francisco & London, 1975. Chap. 10.
[41] J. Tersoff, Empirical interatomic potential for carbon, with applications to amorphous carbon, Physics Review Letters 61 (1988) 2879–2882.
[42] S. Torquato, Random Heterogeneous Materials: Microstructure and Macroscopic Properties, Springer-Verlag, New York, 2002.
[43] S. Torquato, Inverse optimization techniques for targeted self-assembly, Soft Matter 5 (2009) 1157.
[44] B. Widom, Random sequential addition of hard spheres to a volume, Journal of Chemical Physics 44 (1966) 3888–3894.
[45] P. Wriggers, Computational Contact Mechanics, John-Wiley, 2002.
[46] T.I. Zohdi, An adaptive-recursive staggering strategy for simulating multifield coupled processes in microheterogeneous solids, The International Journal of Numerical Methods in Engineering 53 (2002) 1511–1532.
[47] T.I. Zohdi, Computational design of swarms, The International Journal of Numerical Methods in Engineering 57 (2003) 2205–2219.
[48] T.I. Zohdi, Modeling and direct simulation of near-field granular flows, The International Journal of Solids and Structures 42 (2) (2004) 539–564.
[49] T.I. Zohdi, A computational framework for agglomeration in thermo-chemically reacting granular flows, Proceedings of the Royal Society 460 (2052) (2004) 3421–3445.
[50] T.I. Zohdi, Charge-induced clustering in multifield particulate flow, The International Journal of Numerical Methods in Engineering 62 (7) (2005) 870–898.

[51] T.I. Zohdi, Computation of strongly coupled multifield interaction in particle-fluid systems, Computer Methods in Applied Mechanics and Engineering 196 (2007) 3927–3950.
[52] T.I. Zohdi, Introduction to the Modeling and Simulation of Particulate Flows, SIAM (Society for Industrial and Applied Mathematics), 2007.
[53] T.I. Zohdi, Mechanistic modeling of swarms, Computer Methods in Applied Mechanics and Engineering 198 (21–26) (2009) 2039–2051.
[54] T.I. Zohdi, On the dynamics of charged electromagnetic particulate jets, Archives of Computational Methods in Engineering 17 (2) (2010) 109–135.